



Article

A Novel Design of Spike-Shaped Miniaturized 4×4 MIMO Antenna for Wireless UWB Network Applications Using Characteristic Mode Analysis

Ankireddy Chandra Suresh ¹, Thatiparthi Sreenivasulu Reddy ¹, Boddapati Taraka Phani Madhav ² , Samah Alshathri ^{3,*} , Walid El-Shafai ^{4,5} , Sudipta Das ^{6,*} and Vishal Sorathiya ⁷

- ¹ Department of Electronics and Communication Engineering, Sri Venkateswara University College of Engineering, SV University, Tirupathi 517502, Andhra Pradesh, India
 - ² Antennas and Liquid Crystals Research Center, Department of Electronics and Communication Engineering, Koneru Lakshmaiah Education Foundation, Guntur 522302, Andhra Pradesh, India
 - ³ Department of Information Technology, College of Computer and Information Sciences, Princess Nourah bint Abdulrahman University, P.O. Box 84428, Riyadh 11671, Saudi Arabia
 - ⁴ Security Engineering Lab, Computer Science Department, Prince Sultan University, Riyadh 11586, Saudi Arabia
 - ⁵ Department of Electronics and Electrical Communications Engineering, Faculty of Electronic Engineering, Menoufia University, Menouf 32952, Egypt
 - ⁶ Department of Electronics and Communication Engineering, IMPS College of Engineering and Technology, Malda 732103, West Bengal, India
 - ⁷ Faculty of Engineering and Technology, Parul Institute of Engineering and Technology, Parul University, Waghodia Road, Vadodara 391760, Gujarat, India
- * Correspondence: sealshathry@pnu.edu.sa (S.A.); sudipta.das1985@gmail.com (S.D.)

Abstract: In this article, a 4×4 miniaturized UWB-MIMO antenna with reduced isolation is designed and analyzed using a unique methodology known as characteristic mode analysis. To minimize the antenna's physical size and to improve the isolation, an arrangement of four symmetrical radiating elements is positioned orthogonally. The antenna dimension is $40 \text{ mm} \times 40 \text{ mm}$ ($0.42\lambda_0 \times 0.42\lambda_0$) (λ_0 is the wavelength at first lower frequency), which is printed on FR-4 material with a width of 1.6 mm and $\epsilon_r = 4.3$. A square-shaped defected ground framework was placed on the ground to improve the isolation. Etching square-shaped slots on the ground plane achieved the return losses $S_{11} < -10 \text{ dB}$ and isolation 26 dB in the entire operating band $3.2 \text{ GHz} - 12.44 \text{ GHz}$ (UWB ($3.1 - 10.6 \text{ GHz}$) and X-band ($8 \text{ GHz} - 12 \text{ GHz}$) spectrum and achieved good isolation bandwidth of 118.15% . The outcomes of estimated and observed values are examined for MIMO inclusion factors such as DG, ECC, CCL, and MEG. The antenna's performances, including radiation efficiency and gain, are remarkable for this antenna design. The designed antenna is successfully tested in a cutting-edge laboratory. The measured outcomes are quite similar to the modeled outcomes. This antenna is ideal for WLAN and Wi-Max applications.

Keywords: characteristic mode analysis; defected ground system; envelop correlation coefficient; isolation; MIMO; UWB; X-band



Citation: Suresh, A.C.; Reddy, T.S.; Madhav, B.T.P.; Alshathri, S.; El-Shafai, W.; Das, S.; Sorathiya, V. A Novel Design of Spike-Shaped Miniaturized 4×4 MIMO Antenna for Wireless UWB Network Applications Using Characteristic Mode Analysis. *Micromachines* **2023**, *14*, 612. <https://doi.org/10.3390/mi14030612>

Academic Editors: Ahmed A. Ibrahim and Syed Muzahir Abbas

Received: 24 January 2023
Revised: 23 February 2023
Accepted: 27 February 2023
Published: 7 March 2023



Copyright: © 2023 by the authors. Licensee MDPI, Basel, Switzerland. This article is an open access article distributed under the terms and conditions of the Creative Commons Attribution (CC BY) license (<https://creativecommons.org/licenses/by/4.0/>).

1. Introduction

It is desirable to employ this modern technology, known as Ultra-wideband communication devices, to address the needs of high data rates at low costs. Since the Federal Communications Commission (FCC) approved the unlicensed $3.1 \text{ GHz} - 10.6 \text{ GHz}$ range for UWB applications; it has evolved into a well-known innovation in the wireless communication industry. Because they constitute an essential part of UWB communication systems, UWB antennas have consequently generated enormous scholarly and scientific attention in recent years [1]. A technological breakthrough known as UWB allows for reliable wireless connectivity with greater capacity and data speeds. However, UWB has limited short-range

characteristics as a result of how low power is handled. Due to congestion issues with fading, multipath mitigation, and low power handling capabilities, UWB is thus limited to residential applications [2]. To overcome the issues mentioned above, the MIMO technique was combined with UWB technology. Higher bandwidth and data rates are possible with MIMO technology while raising total sent power. By using proper and appropriate antenna elements at both ends of the communication system, the maximum energy efficiency of the communication system can be achieved without affecting the power capacities of the communication system. Given that we can simply replace the MIMO parts while the transmitted power stays constant, we should arrange the appropriate MIMO antennas to increase channel capacity [3].

Introducing more components causes mutual coupling to rise, which lowers MIMO's performance. Since electromagnetic interaction increases when MIMO units are put closely together and lowers MIMO performance, low mutual coupling is a crucial MIMO component. These techniques are used to initiate reducing mutual coupling: (1) an improper ground structure, (2) networks for decoupling, (3) parasitic components, (4) electromagnetic band gap (EBG), (5) lines of neutralization, and (6) meta material. To fulfill the expectations of the Internet of Things for more bandwidth and data rates, researchers have started to create UWB antennas to attain a high level of isolation in MIMO Antennas [4]. Two circular patches that are orthogonal to one another constitute the antenna. Two notched bands can be generated by combining a y-shaped slot, a rectangular slot, and a circumferential slot [5]. Innovative approaches are developed for enhancing isolation, bandwidth, and gain. Regarding IoT applications, bidirectional UWB over a multi-mode link increased data rates to 2 Gbps at a lesser cost [6]. To increase impedance matching and achieve 20 dB isolation, the boundaries of triangular-shaped loadings are embedded with a modified Koch fractal structure in MIMO antennas [7]. The Circular UWB-MIMO antenna demonstrated impressive isolation of 28 dB and IBW 134.68% by utilizing a T-shaped slot and protruding strips [8]. Such components allowed the planned antenna to function between 24.1 GHz and 27.18 GHz and between 33 GHz and 44.13 GHz [9]. A 2×2 double band antenna composed of the optically reflecting surface AgHT 8 has been planned for use in Wireless LAN and Area network operations [10]. A 4×4 planer UWB was created employing circular monopoles as radiators, and isolation was enhanced using DGS and EBG structures. This modified EBG, mushroom shape produced the isolation of more than 17.5 dB across the whole frequency range of 3.0 to 16.2 GHz [11].

The 4×4 small antennas have 25 mm \times 50 mm of surface area, and PIN diodes were utilized to turn on each radiator in the set up. An LC-shaped decoupling stub was employed for high isolation (2–12 GHz) across the band [12]. A 4×4 spike Ultra-wideband antenna with a 50 mm \times 25 mm footprint uses dropouts to block Wireless LAN bands between 4.9 GHz and 6.4 GHz. This antenna maintains good isolation from 2 GHz to 12 GHz. All four components for polarization diversity are in opposition to one another. An LC decoupling stub was employed to increase isolation and decrease ECC [13]. A tiny circular-shaped 4×4 UWB-MIMO has the following measurements: $44 \times 44 \times 1.6$ mm³, and each radiator has a U-shaped slot. Excellent isolation and diversity measurements were attained [14] as a result of the crescent slot on the circular radiator and the circular slot resonator. Using the 4×4 rectangle MIMO antenna with an arrow-shaped etching on the rectangular patch, the isolation was increased by more than 18 dB [15]. A two-port UWB-MIMO antenna with semi-circular radiating elements was able to achieve 55 dB isolation and a 37 GHz bandwidth by employing a decoupling stub on the ground. The antenna is 18 mm \times 36 mm \times 1.6 mm, and it was created utilizing the space diversity technique to boost impedance and bandwidth [16]. A new technique was used to create a multi-input multi-output (MIMO) 4×4 elliptical monopoles Ultra-Wide-band (UWB) device with a tiny footprint (45 mm \times 45 mm \times 1.6 mm). An H-shaped slot and a C-shaped slot were combined in this design to provide double band rejection performance at 5.5 GHz and 7.5 GHz. A stub was connected to the edge of each defective ground structure to provide isolation of 22 dB [17]. A compact 4×4 octagonal Koch fractal shape was employed to

attain a modest size. Four radiators were positioned diagonally in the 2 GHz–10.6 GHz frequency range, and grounded stubs were employed to increase isolation by 17 dB [18]. To achieve greater isolation and good radiation performance metrics, researchers applied techniques such as orthogonal, Asymmetric Coplanar Strip (ACS), polarization diversity, space diversity, slotted annular ring, and decoupling stubs [19–25].

But the above methods are not able to enhance the isolation. Therefore, we need an advanced antenna design approach that offers us great isolation and good diversity performance. A method of evaluation that is step-by-step is characteristic mode analysis. This design method is used to analyze antenna properties without using feed. The antenna structure is physically examined using CMA.

The following sections compose the remaining document: In Section 2, the size and design of the antenna are explained. In Section 3, the proposed antenna is tested with the characteristic mode analysis. The simulated and observed findings are discussed in Section 4. In Section 5, the newly created antenna is contrasted with current models. Section 6 concludes the essay.

2. Design of 4 × 4 Spike-Shaped UWB Antenna

The designed antenna radiator is in the form of a spike-shape. The four symmetrical monopoles are placed orthogonal to one other, resulting polarization diversity. The proposed spike-shaped MIMO antenna has size in the order of 40 mm × 40 mm × 1.6 mm ($0.44\lambda_0 \times 0.44\lambda_0 \times 0.0176\lambda_0$), placed on a Fr-4 material with loss tangent of 0.002 and permittivity of 4.3. The Computer Simulation Technology (CST) is used to design and simulate the proposed antenna.

The spike-shaped single radiator is a circular patch with a radius of 4 mm and it has five spike bubbles with a diameter of 1.5 mm placed on its circumference. The feeder line has a width of 1.2 mm, length is of about 10.2 mm, and the distance between two radiators is 6.25 mm. In this design, a novel ground structure shape is used to achieve good radiation performance and better isolation.

All four radiators are of the same dimensions and are arranged in an orthogonal pattern. By using this arrangement of elements in MIMO, it is possible to reduce the mutual coupling among patch elements. Four rectangular-shaped patches with a width of 8.334 mm and a length of 7 mm form the structure of the ground plane. In order to achieve good isolation, a square-shaped conducting patch with a width of 3 mm is placed on the ground at a distance of 5 mm from the center of ground plane, as shown in Figure 1b. To improve the bandwidth and isolation in UWB and ITU bands, 12 rectangular slots are placed on 3 mm square ground patch.

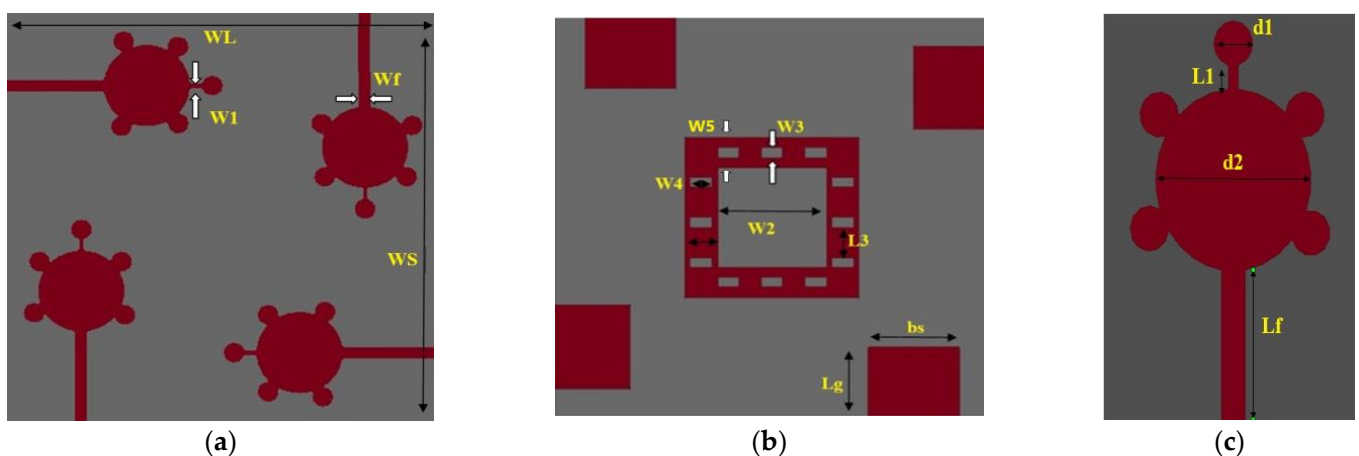


Figure 1. Orientation of the designed antenna (a) top view, (b) bottom view, (c) single element.

Out of those 12 rectangular slots, 6 slots are placed vertically, and the remaining slots are placed horizontally on a square-shaped ground patch as shown in Figure 1b. The dimensions of a 4×4 spike-shaped Ultra-wide band antenna are shown in Table 1.

Table 1. Dimensions of spike-shaped 4×4 UWB-MIMO.

Parameter	Symbol	Value (mm)	Parameter	Symbol	Value (mm)
Substrate length	W_L	40	Substrate width	W_s	40
Length of the spike ground	L_1	2	Ground length	L_g	8.33
Radiator diameter	d_2	8	Feed length	L_f	10.2
Diameter of spike	d_1	1	Width of the square ground patch	L_1	3
Feed width	W_f	1.2	Space between two vertical slots	L_3	3
Square patch length	W_2	10	Width of the ground	bs	7
Width of the slot	W_4	2	Width of square patch	W_5	3
Height of the slot	W_3	1			

Theory of Characteristic Mode Analysis

Characteristic mode theory is used to analyze the antenna's input impedance and current distributions without any excitation. The characteristic mode theory (CMT) is used to study radiation patterns and scattering fields in perfect electric conductors. In perfect electric conductors, the antenna's input impedance and radiation pattern are proportional to the total surface current density at the feeding point [26]. The impedance matrix is represented in the below equation.

$$z_{imp} = R_{real} + jI_{img} \quad (1)$$

$$[I]j_n = \lambda_n [R] j_n \quad (2)$$

where R is the real part and I is the imaginary part of impedance matrix. Here λ_n denotes the Eigen Vector's eigenvalues. J_n is the antenna current defined in terms of its characteristic modes

$$j_n = \sum_n^N \frac{J_n E^i}{1 + j\lambda_n} = \sum_n^N \alpha_n J_n \quad (3)$$

where N is the order of the moment matrix and J_n is CM current, λ_n eigen values and E^i is incident electric field. Equation (1) explains the characteristic modes in the antenna structure. Equation (1) has two terms $J_n E^i$ and $\frac{1}{1+j\lambda_n}$.

The dot product of E^i and J_n is zero at all points except the feed point of the conducting antenna. The overall phase of E^i depends on eigen values λ_n .

3. Evaluation Procedure of 4×4 UWB-MIMO Antenna

The characteristics mode analysis (CMA) is used to develop the proposed antenna. The entire design process is carried out in four design stages performed in the proposed antenna design evaluation process. The total designing process of the suggested antenna depends on CMA metrics such as (1) Eigen values, (2) characteristic angle, and (3) modal significance. These three properties exist in each characteristic mode. In this current antenna design, only the modal significance parameter was considered. The Spike-shaped 4×4 MIMO antenna is analyzed and investigated in four stages: antenna0 (Ant#0), antenna1 (Ant#1), antenna2 (Ant#2), and antenna3 (Ant#3) [27]. The CM currents in CMA are used to evaluate the performance of each characteristic mode. Without using any excitation, these characteristic mode current distributions can be observed. The proposed antenna achieved a good

impedance bandwidth (IBW) covering the bandwidth requirements of UWB systems and also X-band.

The proposed antenna was developed using a CMA method. A series of sequential procedures are used throughout the designing process. The modal current distribution in Computer Simulation Technology (CST) is demonstrated using multi-layer solver. The evaluation process of antenna in step-by-step manner is depicted in Figure 2

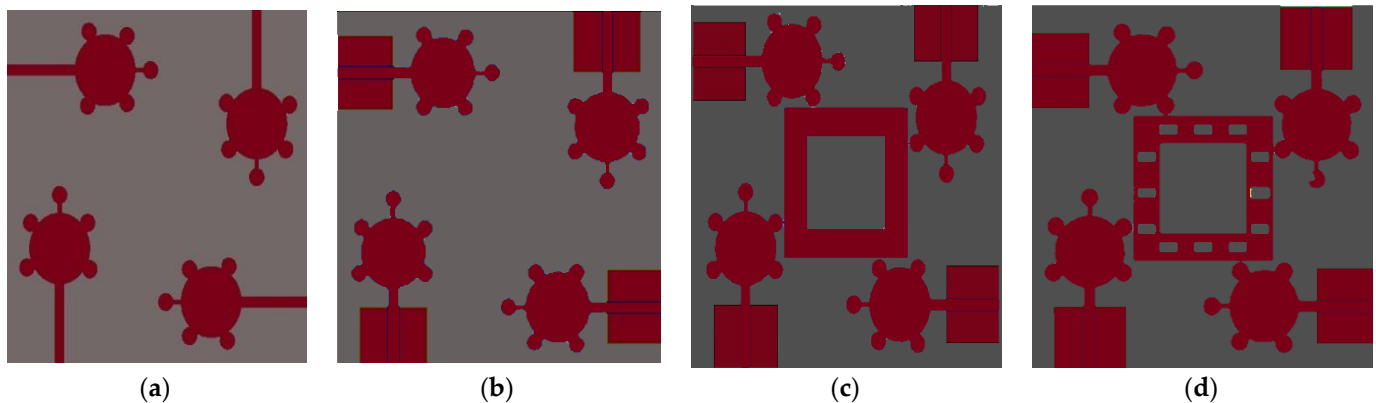


Figure 2. Step by step design procedure of spike antenna. (a) Ant#0 (b) Ant#1 (c) Ant#2 (d) Ant#3.

Modal significance is used to implement the proposed antenna in CMA design. Without using any excitation signal, the entire antenna design process is carried out in four evaluation stages from Ant#0 to Ant#3. The Ant#0 is made up of four spike-shaped radiators that are printed on FR-4 substrate. Each spike radiator has a radius of 4 mm with spike bubble radius of 1 mm. The Ant#0 has no conducting ground plane and is able to generate ten characteristic modes using the multilayer solver. Only five out of ten characteristic modes (CMs) contribute bandwidth and isolation. The modal significances of Ant#0 are shown in Figure 3a. The characteristics modes CM1, CM2, CM4, CM5, and CM6 contribute bandwidth between 4 GHz and 6 GHz. The remaining modes CM3, CM7, CM8, CM9, and CM10 do not contribute any bandwidth. The Ant#0 is good at mid-band frequencies (4 GHz–6 GHz) and not good at low and high frequencies. In Ant#0, the absence of a ground plane produces high mutual coupling at low and high frequencies. Ant#0's design was changed to improve isolation and bandwidth. On the ground plane, rectangular ground edges were added for each radiator. The rectangular ground edges are 8.33 mm and 7 mm in width and length, respectively. Hence, Ant#0 becomes Ant#1 after the ground edges are added. Ant#1's characteristic modes were examined in the absence of excitation. Ant#1 generates ten different modes. The majority of the characteristics modes, CM1, CM2, CM4, and CM6, are concentrated at mid frequencies (4 GHz–8 GHz) while CM5 and CM10 are concentrated in between 8 GHz and 11 GHz. The remaining modes, CM3, CM7, CM8, and CM9, are ineffective and contribute no bandwidth and isolation, this is due to the addition of ground edges in the ground plane. Figure 3 depicts the corresponding modal significances on the ground plane, a 3 mm square-shaped conducting patch is added to convert Ant#1 to Ant#2 and analyze its characteristic modes. Some CMs are below 4.5 GHz, some are at mid-band frequencies, and some are at 11 GHz, implying that this antenna achieved good bandwidth but requires more isolation. In Figure 3c, the corresponding modal significances of Ant#2 are shown. Ant#2 was transformed into Ant#3 by adding 12 rectangular slots on 3 mm square patch in ground plane. Ant#3 can be examined in terms of its characteristic modes. The CM3 and CM7 does not contribute any bandwidth in the ten modes.

The remaining modes, CM1, CM2, CM4, CM5, CM6, CM8, CM9, and CM10, not only covers UWB but also the X-band (8 GHz–12 GHz). Figure 3d shows the corresponding modal significances. The CM4 is resonated at 4.1 GHz during the evaluation process from Ant#0 to Ant#3. As a result, CM4 is referred to as the dominant mode. All CMs are scattered

in between 3 GHz and 12 GHz except CM3 and CM7. The feed is applied to all antennas and their corresponding S-Parameters are depicted in Figure 4. Placing the square-shaped ground structure in the proposed antenna, the current interactions among the radiators reduce because of the increase in current interaction between the ground conduction patch and radiators.

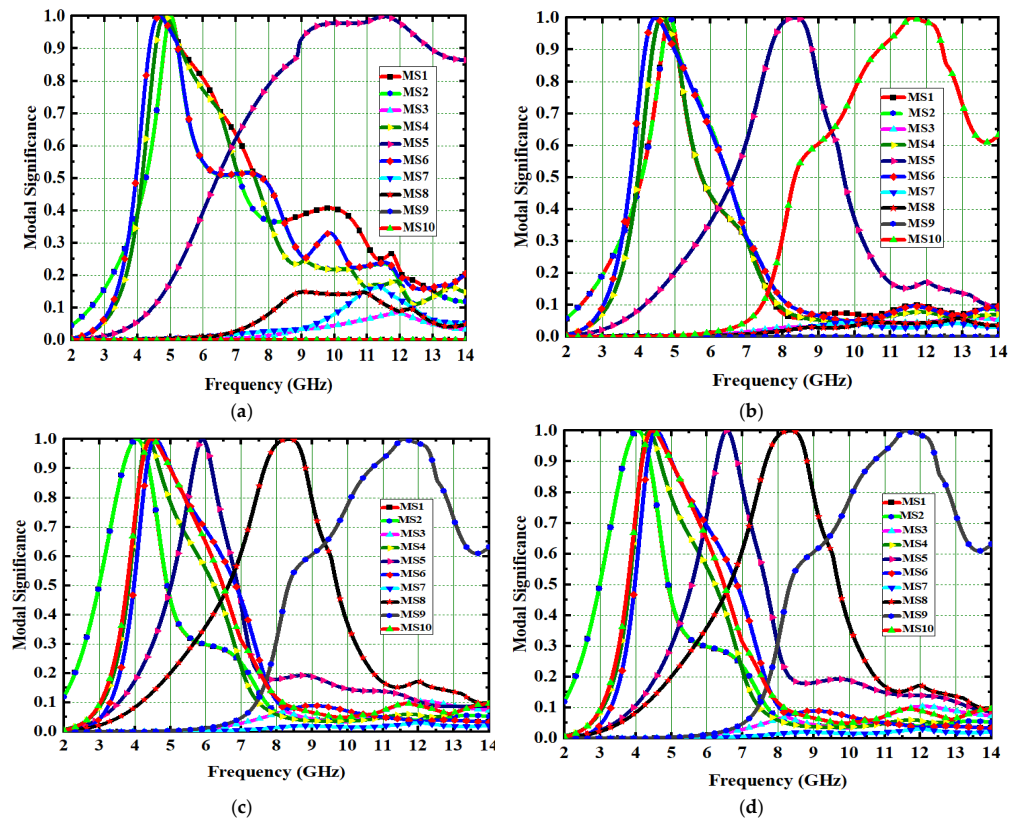


Figure 3. Spike antenna model significances. (a) Ant#0, (b) Ant#1, (c) Ant#2, (d) Ant#3.

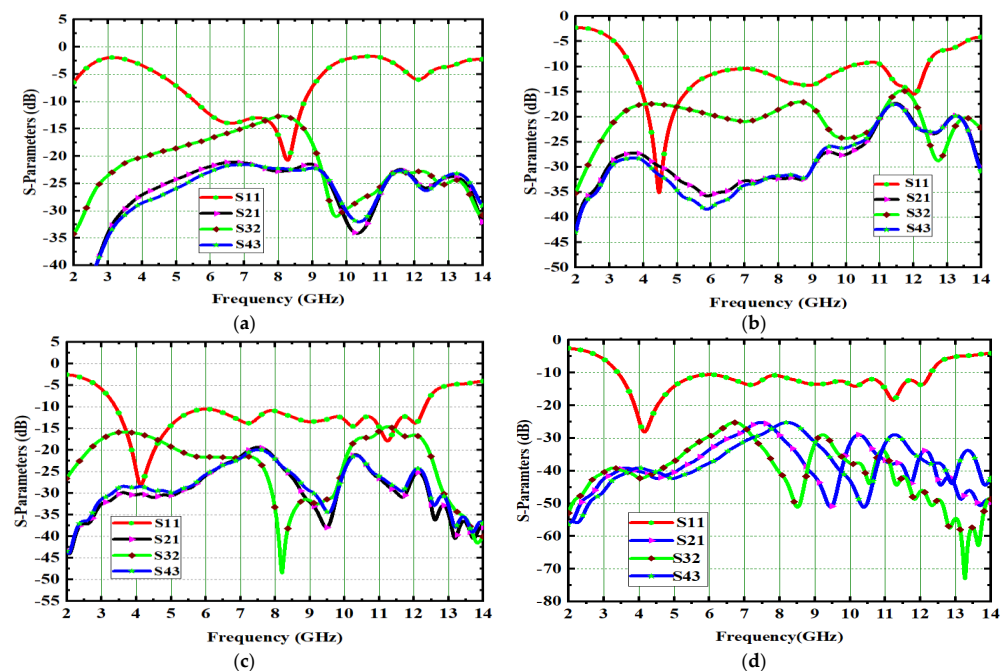


Figure 4. Spike antenna S-parameters. (a) Ant#0, (b) Ant#1, (c) Ant#2, (d) Ant#3.

This antenna is suitable for UWB (3.1–10.6 GHz) and X-band applications (8–12 GHz). Figures 5–8 shows the characteristic current distributions of antennas Ant#0 to Ant#3 at 4.1 GHz, 7.2 GHz, and 10.1 GHz. Figure 9 shows Ant#3's current distributions at various frequencies.

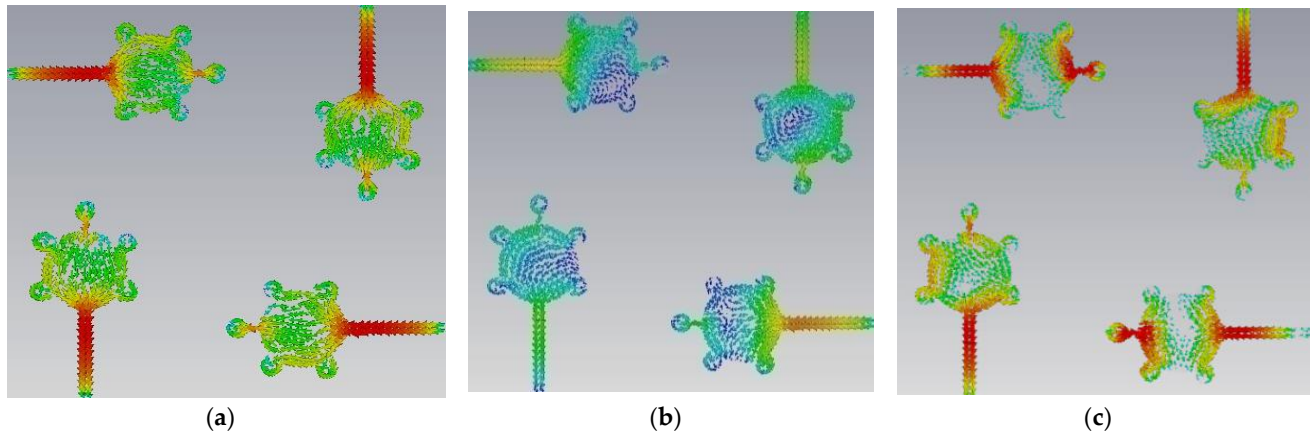


Figure 5. Current distribution effects on spike antenna at different frequencies in CM4 at (a) 4.1 GHz, (b) 7.2 GHz, (c) 10.1 GHz.

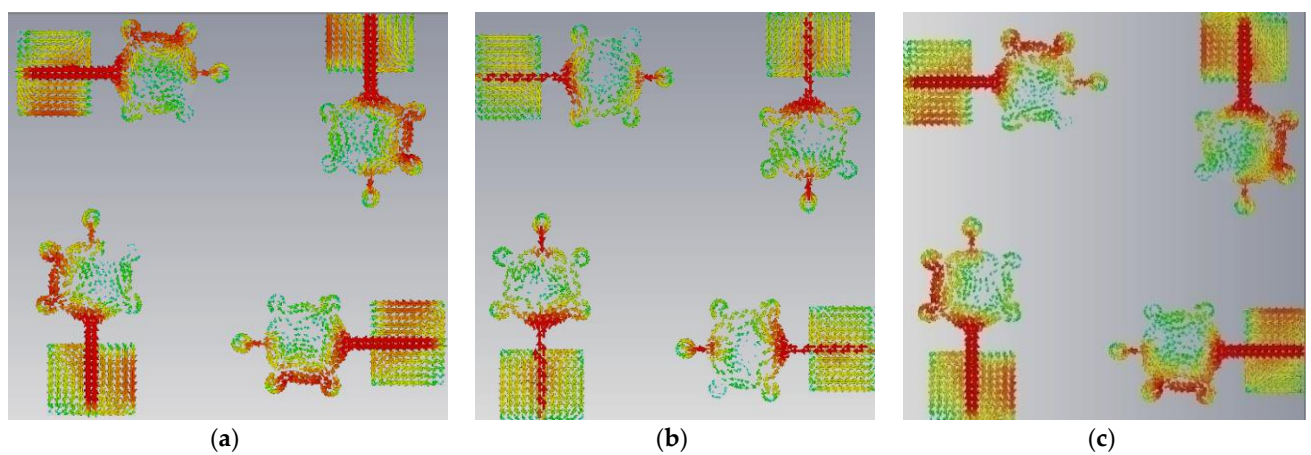


Figure 6. Current distribution effects on spike antenna at different frequencies for CM4 in Ant#0 at (a) 4.1 GHz, (b) 7.2 GHz, (c) 10.1 GHz.

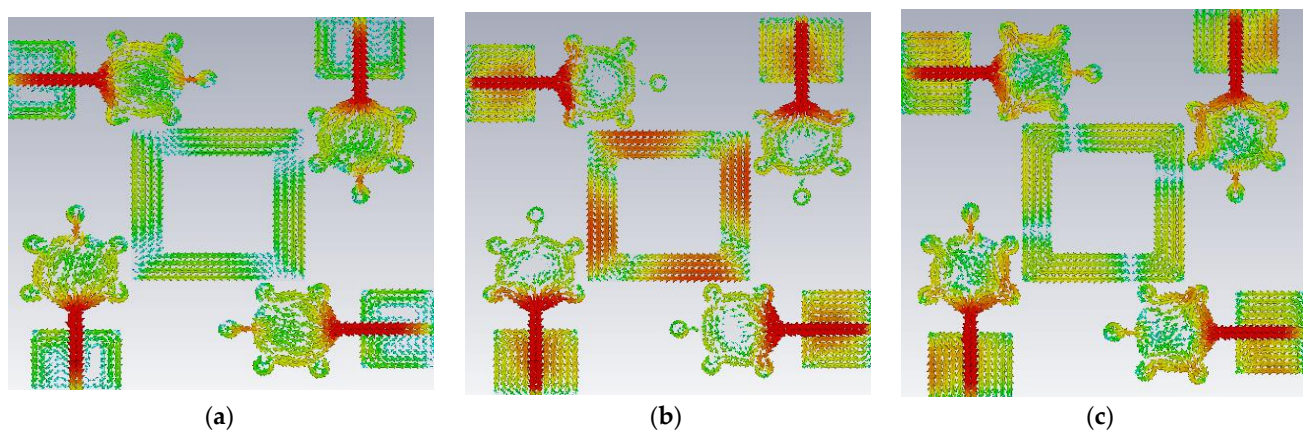


Figure 7. Current distribution effects on spike antenna at different frequencies for CM4 in Ant#1 at (a) 4.1 GHz, (b) 7.2 GHz, (c) 10.1 GHz.

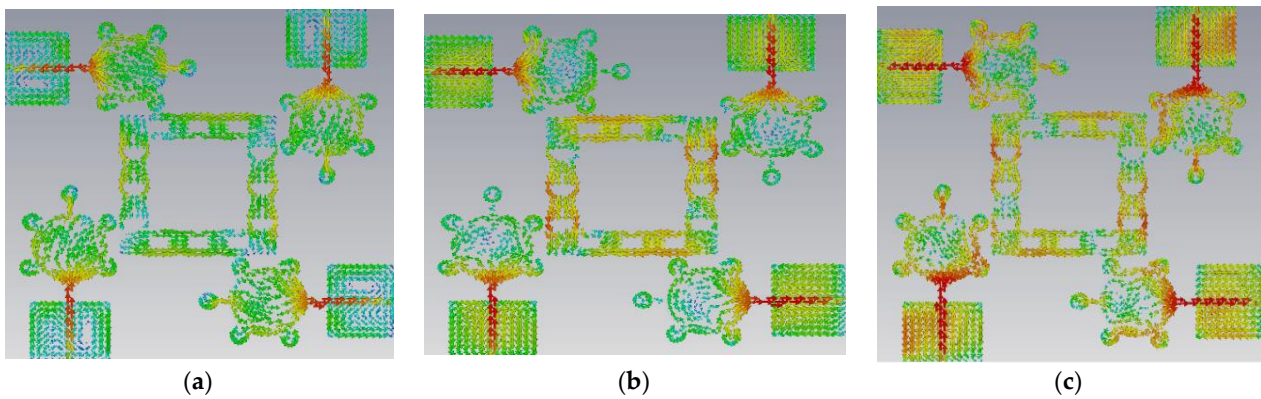


Figure 8. Current distribution effects on spike antenna at different frequencies for CM4 in Ant# 2 at (a) 4.1 GHz, (b) 7.2 GHz, (c) 10.1 GHz.

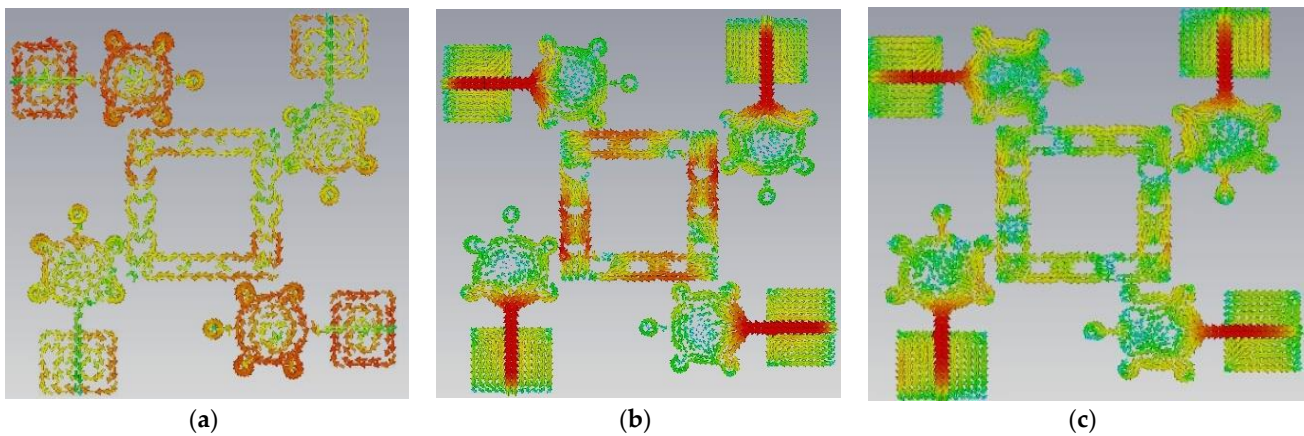


Figure 9. Current distribution effects on spike antenna at different frequencies for CM4 in Ant#3 at (a) 4.1 GHz, (b) 7.2 GHz, (c) 10.1 GHz.

4. Results of 4×4 Spike-Shaped UWB-MIMO Antenna

The proposed UWB-MIMO spike-shaped antenna has good MIMO metrics such as radiation characteristics and isolation. The CMA technique is used to design the spike-shaped antenna, resulting in improved isolation. From 3.2 GHz to 12.44 GHz, the impedance bandwidth is 9.24 GHz and it covers the bandwidth requirements for UWB and ITU bands. Figure 10 depicts the designed antenna prototype. The experimental set up for measuring the reflection coefficient using VNA is shown in Figure 11a. Figure 11b compares both the simulated and measured reflection coefficients (S_{11}). The designed antenna provides isolation of 26 dB. This isolation is good in MIMO antenna metrics. The experimental set up for measuring the isolation using VNA is shown in Figure 12a. Figure 12b provides a comparative analysis of simulated and experimental S_{21} values. The novel type of decoupling structure in the ground plane provides the excellent isolation.

Figure 13 shows the 4×4 radiation patterns at 4.1 GHz, 7.2 GHz, and 10.1 GHz. The E-plane and H-plane of the primary radiator are obtained by activating its port and other ports are connected with 50 ohm load. An anechoic chamber set up is used to measure the radiation pattern, with the aid of the DRH20. The radiation efficiency is achieved as 89% and gain is 4.9 dB as shown in Figure 14.



Figure 10. Fabricated prototype model of proposed spike antenna (a) front view, (b) back view.

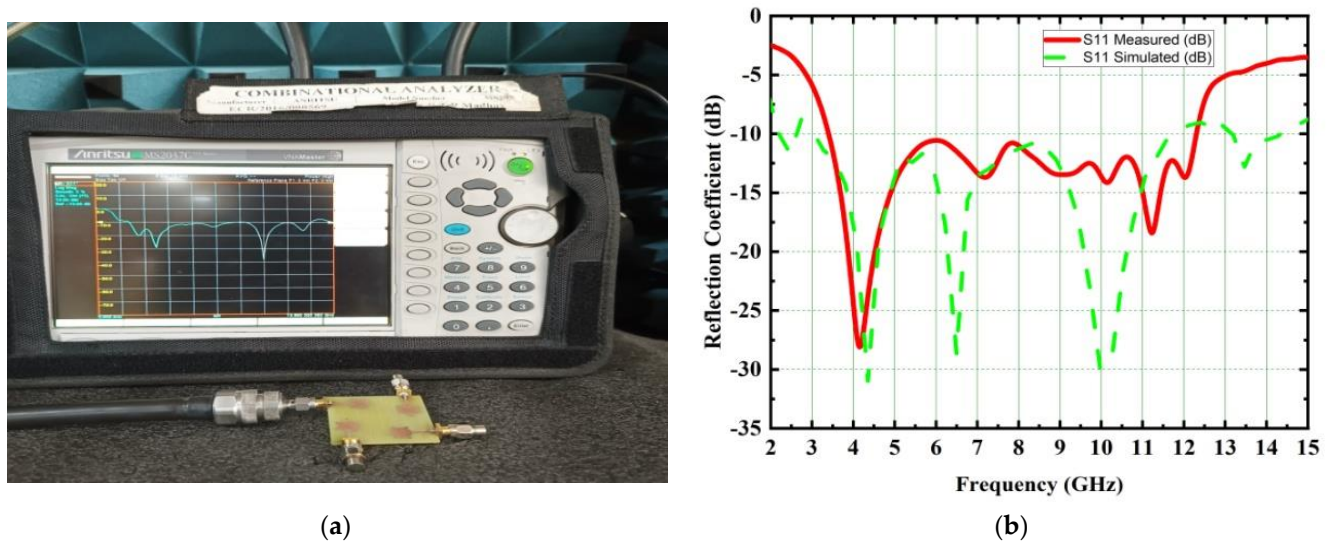


Figure 11. Simulated and measured reflection coefficients of the proposed spike antenna (a) S_{11} measurement set up using VNA, (b) simulated and measured S_{11} comparison.

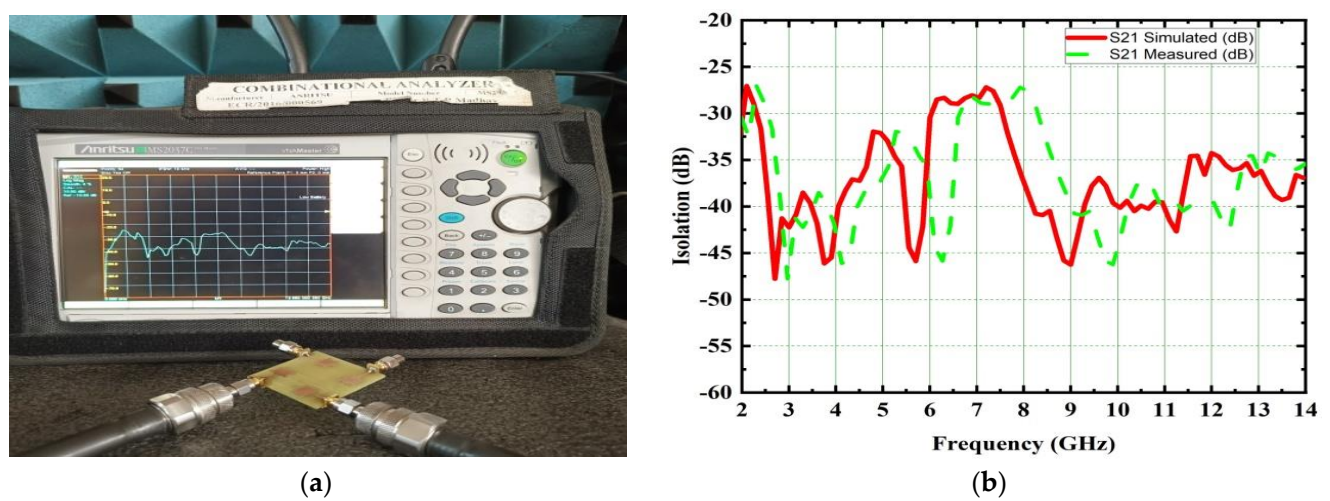


Figure 12. Simulated and measured isolation characteristics of the proposed spike antenna (a) S_{21} measurement set up using VNA (b) simulated and measured S_{21} comparison.

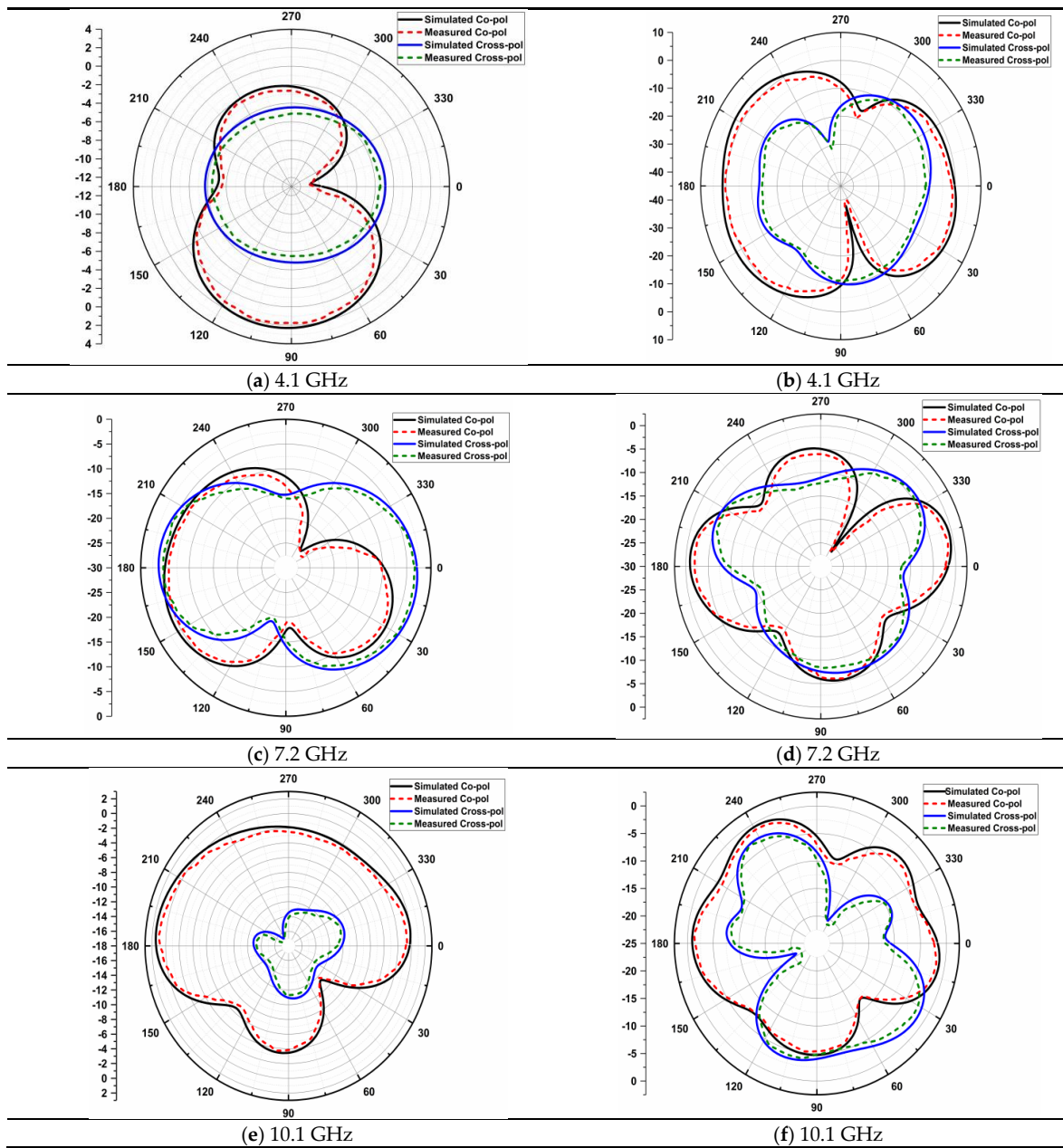


Figure 13. Radiation patterns of spike antenna at various frequencies in E (a,c,e) and H (b,d,f)—planes.

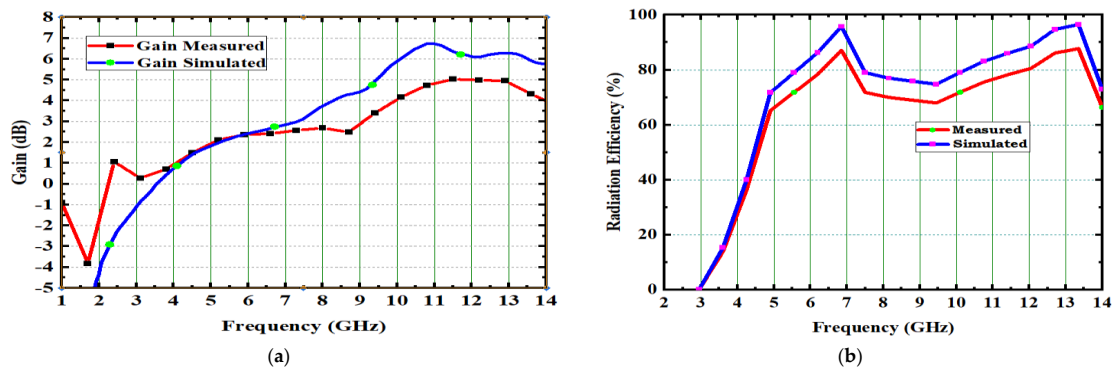


Figure 14. Gain and radiation efficiency of spike antenna. (a) Gain vs. Frequency. (b) Radiation Efficiency vs. Frequency.

4.1. Spike-Shaped UWB-MIMO Antenna Performance

Four performance metrics exist in MIMO antenna systems, all of which should be acceptable [28–30]. The envelope correlation coefficient is among the key diversity factors for assessing MIMO performance. The ECC describes the interactions between the MIMO elements, it should be ideally zero. Over this operating band, a value of less than 0.5 is acceptable. S-parameters and far-fields can be used to calculate the ECC. The following equation can be used to represent the ECC [28].

$$\rho_{ij} = \frac{|S_{kk}^* S_{km} + S_{mk}^* S_{mm}|^2}{(1 - (|S_{kk}|^2 + |S_{mk}|^2))(1 - (|S_{mm}|^2 + |S_{km}|^2))} \tag{4}$$

where $k = 1$ and $m = 2$. Using sophisticated decoupling methods and characteristic mode analysis this antenna achieved ECC of 0.0016 and is depicted in Figure 15b. The lesser ECC value means the antenna elements were well-isolated in MIMO. The envelope correlation coefficient (ECC) is also computed from far fields [29] and shown in Equation (5).

$$P_e = \frac{\left| \int_0^{2\pi} \int_0^\pi (XPR.E_{\theta 1}.E_{\theta 2}^* P_\theta + E_{\phi 1} E_{\phi 2}^* . P_\phi) d\Omega \right|^2}{\int_0^{2\pi} \int_0^\pi (XPR.E_{\theta 1}.E_{\theta 1}^* P_\theta + E_{\phi 1} E_{\phi 1}^* . P_\phi) d\Omega \int_0^{2\pi} \int_0^\pi (XPR.E_{\theta 2}.E_{\theta 2}^* P_\theta + E_{\phi 2} E_{\phi 2}^* . P_\phi) d\Omega} \tag{5}$$

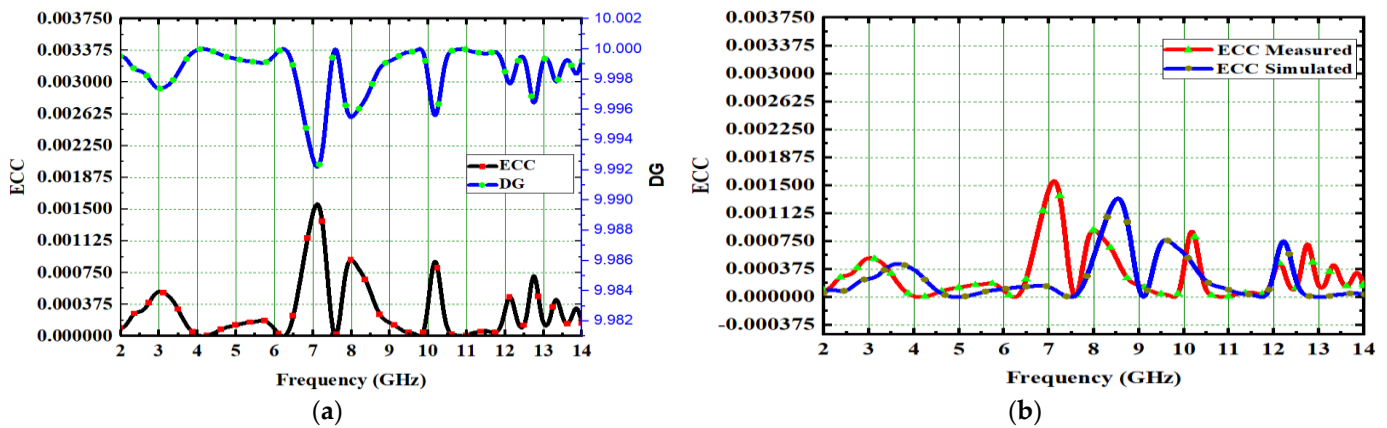


Figure 15. Spike antenna (a) DG and ECC, (b) ECC measured and simulated.

Another important MIMO diversity parameter is diversity gain (DG). Generally, in MIMO antennas the DG is nearly 10 dB. Formula [28] illustrates how such DG is stated in regards of ECC.

$$DG = 10\sqrt{1 - ECC^2} \tag{6}$$

Figure 15a shows that the DG is nearly 9.962 dB. The channel capacity loss (CCL) is another important diversity parameter [30]. The number of elements in a MIMO system determines its channel capacity. In the equation, the CCL [31] is expressed as:

$$CCL = -\log_2 \det(\psi^R) \tag{7}$$

$$\psi^R = \begin{bmatrix} \rho_{11} & \rho_{12} & \rho_{13} & \rho_{14} \\ \rho_{21} & \rho_{22} & \rho_{23} & \rho_{24} \\ \rho_{31} & \rho_{32} & \rho_{33} & \rho_{34} \\ \rho_{41} & \rho_{42} & \rho_{43} & \rho_{44} \end{bmatrix}$$

$$\rho_{ii} = 1 - (|S_{ii}|^2 + |S_{ij}|^2) = -|S_{ii}^* S_{ij} + S_{ji}^* S_{ij}|, \text{ for } i, j = 1 \text{ to } 4$$

The acceptable value of CCL is 0.4 bits/s/Hz. In this proposed design, CCL of 0.31 bits/s/Hz is achieved and depicted in Figure 16a.

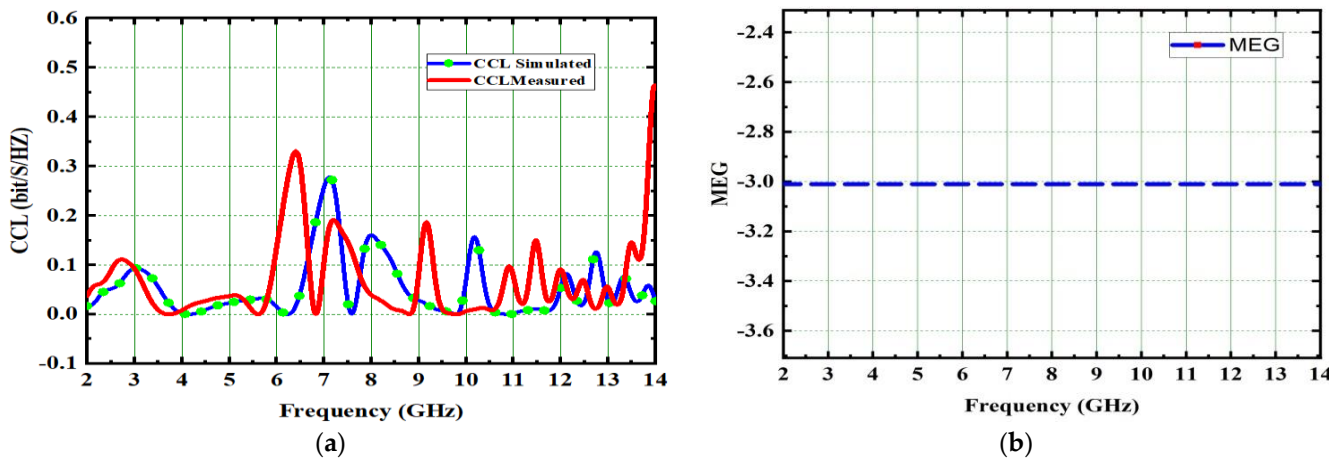


Figure 16. Spike antenna (a) CCL, (b) MEG.

4.2. Mean Effective Gain (MEG)

The MEG can be expressed using Equation (8) [32]

$$MEG_i = \int_0^{2\pi} \int_0^\pi \left[\frac{\hat{r}}{1 + \hat{r}} G_\theta(\theta, \Phi) P_\theta(\theta, \Phi) + \frac{\hat{r}}{1 + \hat{r}} G_\phi(\theta, \Phi) P_\phi(\theta, \Phi) \right] \sin\theta d\theta d\Phi \quad (8)$$

where \hat{r} is the event field's trans discrimination (XPD). The gain components are represented as G_θ and G_ϕ for i^{th} elements. The MEG of the intended antenna is -3.1 dB, as illustrated in Figure 16b.

5. Comparison with Existing Models

The spike-shaped 4×4 UWB-MIMO antenna is designed to work in both UWB and X-band. This antenna has some better features than others previously reported in the literature [11,15,21,24,25,31,32] and illustrated in Table 2. Compared with other conventional models the designed antenna has the added benefit of the CMA process. In the designed UWB-MIMO antenna, the ECC, IBW, and diversity performances are found to be good.

Table 2. Performance comparison of the proposed extended-UWB-MIMO antenna with state-of-the-art antennas.

Ref	Dimensions (mm ³)	Impedance Bandwidth (GHz)	Isolation (dB)	Gain (dB)	Radiation Efficiency (%)	ECC
[11]	$0.55\lambda \times 0.55 \times 0.16\lambda$	3–16.2	>17.5	8.4	>80	<0.3
[15]	$0.69\lambda \times 0.69\lambda \times 0.00\lambda$	2.6–11	>17.4	3.99	>85.7	<0.004
[21]	$0.38\lambda \times 0.38\lambda \times 0.017\lambda$	3.2–11	>15	4	>70	<0.5
[24]	$0.41\lambda \times 0.44\lambda \times 0.01\lambda$	3.1–10.6	>20	4	>90	<0.2
[25]	$0.55\lambda \times 0.55\lambda \times 0.015\lambda$	2.84–15.88	>16	6.35	>89	<0.07
[31]	$0.56 \lambda \times 0.39 \lambda$	3.52–10.08	>22	2.91	—	<0.04
[32]	$0.67 \lambda \times 0.67 \lambda$	2.8–13.3	>18	6	—	<0.06
Prop.	$0.44\lambda \times 0.44\lambda \times 0.0176\lambda$	3.2–12.44	>26	4.9	>89	<0.0016

6. Conclusions

The spike-shaped UWB-MIMO antenna operates in the 3.2 GHz–12.44 GHz frequency range, which includes the entire UWB (3.1 GHz–10.6 GHz) and X-band (8 GHz–12 GHz). Four spike-shaped circular patch radiators are placed orthogonally to achieve polarization diversity. The reflection coefficients (S_{11}) are below -10 dB, and isolation between both the radiating elements are far better than 26 dB. The radiation parameters include 89% radiation efficiency, 118.15% impedance bandwidth, and a 4.9 dB gain. ECC, DG, MEG, and CCL have diversity features of 0.0016, 9.962 dB, -3.1 dB, and 0.31 bits/s/Hz, accordingly. In a cutting-edge experiment, these findings are verified. According to its performance parameters, the developed antenna is suitable for wireless communication in the spectrum of UWB and X-band.

Author Contributions: Conceptualization: A.C.S., T.S.R., B.T.P.M. and S.D.; methodology: A.C.S., S.D., T.S.R. and B.T.P.M.; Formal analysis: S.D., V.S., B.T.P.M.; software: A.C.S., T.S.R., W.E.-S., V.S. and S.A.; validation: A.C.S., S.D., S.A., W.E.-S. and V.S.; writing—original draft preparation: A.C.S., B.T.P.M., T.S.R. and S.D.; writing—review and editing: V.S., S.A. and W.E.-S.; supervision: B.T.P.M. and T.S.R.; Project administration: W.E.-S.; Funding acquisition: S.A. All authors have read and agreed to the published version of the manuscript.

Funding: This work is supported by Princess Nourah bint Abdulrahman University Researchers Supporting Project number (PNURSP2023R197), Princess Nourah bint Abdulrahman University, Riyadh, Saudi Arabia.

Institutional Review Board Statement: Not applicable.

Informed Consent Statement: Not applicable.

Data Availability Statement: The data presented in this research are available on request from the corresponding author.

Acknowledgments: The authors would like to acknowledge Princess Nourah bint Abdulrahman University Researchers Supporting Project number (PNURSP2023R197), Princess Nourah bint Abdulrahman University, Riyadh, Saudi Arabia.

Conflicts of Interest: The authors declare no conflict of interest.

References

1. Sampath, R.; Krishnasamy, T. Selvan Compact hybrid Sierpinski Koch fractal UWB-MIMO antenna with pattern diversity. *Int. J. RF Microw. Comput.-Aided Eng.* **2019**, *30*, e22017. [\[CrossRef\]](#)
2. Kaiser, T.; Zheng, F.; Dimitrov, E. An overview of ultra-wide-band systems with MIMO. *Proc. IEEE* **2009**, *97*, 285–312. [\[CrossRef\]](#)
3. Singal, A.; Kedia, D. Energy efficiency analysis of antenna selection techniques in Massive MIMO-OFDM system with hardware impairments. *J. Comput. Netw. Commun.* **2018**, *2018*, 6131247. [\[CrossRef\]](#)
4. Radhi, A.H.; Nilavalan, R.; Wang, Y.; Al-Raweshidy, H.S.; Eltokhy, A.A.; Ab Aziz, N. Mutual coupling reduction with a wideband planar decoupling structure for UWB-MIMO antennas. *Int. J. Microw. Wirel. Technol.* **2018**, *10*, 1143–1154. [\[CrossRef\]](#)
5. Zhou, J.Y.; Wang, Y.; Xu, J.M.; Du, C. A CPW-fed UWB-MIMO antenna with high isolation and dual band-notched characteristic. *Prog. Electromagn. Res. M* **2021**, *102*, 27–37. [\[CrossRef\]](#)
6. Mirza, J.; Ghafoor, S.; Hussain, A. A full-duplex ultra-wideband over multimode fiber link for internet of things based smart home applications. *Trans. Emerg. Telecommun. Technol.* **2020**, *31*, e4050. [\[CrossRef\]](#)
7. Gorai, A.; Ghatak, R. Utilization of shorted fractal resonator topology for high isolation and ELC resonator for band suppression in compact MIMO UWB antenna. *AEU-Int. J. Electron. Commun.* **2019**, *113*, 152978. [\[CrossRef\]](#)
8. Addepalli, T.; Anitha, V.R. A very compact and closely spaced circular shaped UWB MIMO antenna with improved isolation. *AEU-Int. J. Electron. Commun.* **2020**, *114*, 153016. [\[CrossRef\]](#)
9. Desai, A.; Bui, C.D.; Patel, J.; Upadhyaya, T.; Byun, G.; Nguyen, T.K. Compact Wideband Four Element Optically Transparent MIMO Antenna for mm-Wave 5G Applications. *IEEE Access* **2020**, *8*, 194206–194217. [\[CrossRef\]](#)
10. Desai, A.; Upadhyaya, T.; Palandoken, M.; Gocen, C. Dual band transparent antenna for wireless MIMO system applications. *Microw. Opt. Technol. Lett.* **2019**, *61*, 1845–1856. [\[CrossRef\]](#)
11. Wu, W.; Yuan, B.; Wu, A. A quad-element UWB-MIMO antenna with band-notch and reduced mutual coupling based on EBG structures. *Int. J. Antennas Propag.* **2018**, *2018*, 8490740. [\[CrossRef\]](#)
12. Khan, M.S.; Iftikhar, A.; Shubair, R.M.; Capobianco, A.; Asif, S.M.; Braaten, B.D.; Anagnostou, D.E. Ultra-compact reconfigurable band reject UWB MIMO antenna with four radiators. *Electronics* **2020**, *9*, 584. [\[CrossRef\]](#)

13. Khan, M.S.; Naqvi, S.A.; Iftikhar, A.; Asif, S.M.; Fida, A.; Shubair, R.M. A WLAN band-notched compact four element UWB MIMO antenna. *Int. J. RF Microw. Comput.-Aided Eng.* **2020**, *30*, e22282. [[CrossRef](#)]
14. Sri, G.R.; Rani, A.J.; Saritha, V. Design and Implementation of a Very Compact MIMO Antenna Providing Dual Notches at WLAN and Xband. *Prog. Electromagn. Res. C* **2020**, *104*, 241–252. [[CrossRef](#)]
15. Naktong, W.; Ruengwaree, A. Four-port rectangular monopole antenna for UWB-MIMO applications. *Prog. Electromagn. Res. B* **2020**, *87*, 19–38. [[CrossRef](#)]
16. Irshad Khan, M.; Khattak, M.I.; Rahman, S.U.; Qazi, A.B.; Telba, A.A.; Sebak, A. Design and investigation of modern UWB-MIMO antenna with optimized isolation. *Micromachines* **2020**, *11*, 432. [[CrossRef](#)]
17. Pannu, P.; Sharma, D.K. A low-profile quad-port UWB MIMO antenna using defected ground structure with dual notch-band behavior. *Int. J. RF Microw. Comput.-Aided Eng.* **2020**, *30*, e22288. [[CrossRef](#)]
18. Tripathi, S.; Mohan, A.; Yadav, S. A compact Koch fractal UWB MIMO antenna with WLAN band-rejection. *IEEE Antennas Wirel. Propag. Lett.* **2015**, *14*, 1565–1568. [[CrossRef](#)]
19. Srivastava, K.; Kumar, A.; Kanaujia, B.K.; Dwari, S.; Kumar, S. A CPW-fed UWB MIMO antenna with integrated GSM band and dual band notches. *Int. J. RF Microw. Comput.-Aided Eng.* **2019**, *29*, e21433. [[CrossRef](#)]
20. Ibrahim, A.A.; Abdalla, M.A.; Volakis, J.L. 4 elements UWB MIMO antenna for wireless applications. In Proceedings of the 2017 IEEE International Symposium on Antennas and Propagation & USNC/URSI National Radio Science Meeting, San Diego, CA, USA, 19 October 2017; pp. 1651–1652. [[CrossRef](#)]
21. Mathur, R.; Dwari, S. Compact 4-Port MIMO/diversity antenna with low correlation for UWB application. *Frequenz* **2018**, *72*, 429–435. [[CrossRef](#)]
22. Sipal, D.; Abegaonkar, M.P.; Koul, S.K. Easily extendable compact planar UWB MIMO antenna array. *IEEE Antennas Wirel. Propag. Lett.* **2017**, *16*, 2328–2331. [[CrossRef](#)]
23. Ali, W.A.E.; Ibrahim, A.A. A compact double-sided MIMO antenna with an improved isolation for UWB applications. *AEU-Int. J. Electron. Commun.* **2017**, *82*, 7–13. [[CrossRef](#)]
24. Amin, F.; Saleem, R.; Shabbir, T.; Rehman, S.U.; Bilal, M.; Shafique, M.F. A compact quad-element UWB-MIMO antenna system with parasitic decoupling mechanism. *Appl. Sci.* **2019**, *9*, 2371. [[CrossRef](#)]
25. Balaji, V.R.; Addepalli, T.; Desai, A.; Nella, A.; Nguyen, T.K. An inverted L-strip loaded ground with hollow semi-hexagonal four-element polarization diversity UWB-MIMO antenna. *Trans. Emerg. Telecommun. Technol.* **2022**, *33*, e4381. [[CrossRef](#)]
26. Suresh, A.C.; Reddy, T.S. High Isolation with Fork-Shaped Stub in Compact UWB-MIMO Antenna Using CMA. In Proceedings of the 2021 International Conference on Recent Trends on Electronics, Information, Communication & Technology (RTEICT), Bangalore, India, 27–28 August 2021; pp. 505–511. [[CrossRef](#)]
27. Suresh, A.C.; Reddy, T.S. A Flower Shaped Miniaturized 4×4 MIMO Antenna for UWB Applications Using Characteristic Mode Analysis. *Prog. Electromagn. Res. C* **2022**, *119*, 219–233. [[CrossRef](#)]
28. Sultan, K.S.; Abdullah, H.H. Planar UWB MIMO-diversity antenna with dual notch characteristics. *Prog. Electromagn. Res. C* **2019**, *93*, 119–129. [[CrossRef](#)]
29. Khan, M.S.; Rigobello, F.; Ijaz, B.; Autizi, E.; Capobianco, A.D.; Shubair, R.; Khan, S.A. Compact 3-D eight elements UWB-MIMO array. *Microw. Opt. Technol. Lett.* **2018**, *60*, 1967–1971. [[CrossRef](#)]
30. Farahani, M.; Mohammad-Ali-Nezhad, S. A novel UWB printed monopole MIMO antenna with non-uniform transmission line using nonlinear model predictive. *Eng. Sci. Technol. Int. J.* **2020**, *23*, 1385–1396. [[CrossRef](#)]
31. Tiwari, R.; Singh, P.; Kanaujia, B.; Srivastava, K. Neutralization technique based two and four port high isolation MIMO antennas for UWB communication. *Int. J. Electron. Commun.* **2019**, *110*, 152828. [[CrossRef](#)]
32. Kumar, S.; Gwan, H.; Dong, H.; Wahab, M.; Hyun, C.; Kang, K. Multiple-input-multiple-output/diversity antenna with dual band-notched characteristics for ultra-wideband applications. *Microw. Opt. Technol. Lett.* **2020**, *62*, 336–345. [[CrossRef](#)]

Disclaimer/Publisher’s Note: The statements, opinions and data contained in all publications are solely those of the individual author(s) and contributor(s) and not of MDPI and/or the editor(s). MDPI and/or the editor(s) disclaim responsibility for any injury to people or property resulting from any ideas, methods, instructions or products referred to in the content.